Oral presentation | Reacting flow
Reacting flow
Tue. Jul 16, 2024 2:00 PM - 3:30 PM Room D

[5-D-03] A Compressible Flamelet-Based Turbulent Combustion Modeling Framework in an All-Speed Solver for Rocket Engines

*Siddharth Thakur[1] (1. University of Florida and Streamline Numerics, Inc.)

Keywords: Turbulent Combustion, Compressible Flamelet Model, Rocket Engine

Twelfth International Conference on Computational Fluid Dynamics (ICCFD12), Kobe, Japan, July 14-19, 2024

ICCFD12-2024-C000102

A Compressible Flamelet-Based Turbulent Combustion Modeling Framework in an All-Speed Solver for Rocket Engines

Siddharth Thakur,* Jeffrey Wright and Christopher Neal
Streamline Numerics, Inc., Gainesville, FL, USA

*Corresponding author: st@snumerics.com

Abstract: A computational tool for simulating unsteady turbulent combustion using a compressible flamelet methodology is presented. The objective of this work was to develop a high-performance, high-fidelity simulation capability to enable accurate, fast and robust simulation of unsteady turbulent, reacting flows in rocket engines. The key features of this capability are: (a) compressible flamelet modeling framework for unsteady turbulent combustion and (b) LES and Hybrid RANS-LES (HRLES) methodologies incorporated in a proven existing solver called Loci-STREAM. The standard flamelet methodology is extended to handle both ideal gases and real fluids. The thermodynamics for ideal-gas values is modeled by a linearized specific heat ratio model. Real fluid effects are modeled with the cubic Peng-Robinson equation of state (PR EoS). The parameters needed for the PR EoS are pre-tabulated for the evaluation of departure functions and a quadratic expression as a function of temperature is used to recover the attraction parameter away from the reference temperature. The Compressible Flamelet Progress Variable (CFPV) methodology developed in Loci-STREAM is able to account for pressure and temperature variations from the baseline table and is thermodynamically consistent in the entire flow path of a rocket engine (from oxidizer and fuel manifolds to the exit of the nozzle) and circumvents the need for ad hoc compressibility corrections of the standard Flamelet Progress Variable (FPV) model. These enhancements in Loci-STREAM have yielded higher fidelity and more reliable analytical/design capability relative to existing capability for turbulent reacting flows in rocket engines.

Keywords: Compressible Flamelet Progress Variable model, Peng-Robinson Equation of State, All-Speed Solver

1 Introduction

The use of high-fidelity computational fluid dynamics (CFD) tools early in the product development cycle of rocket engines alleviates testing costs and allows the development of these devices better, faster and cheaper. In the design of advanced propulsion systems, CFD plays a major role in defining the required performance over the entire flight regime, as well as in testing the sensitivity of the design to the different modes of operation. In the present work, a robust and computationally efficient unsteady turbulent compressible combustion modeling capability developed in a CFD solver called Loci-STREAM [1] is presented.

Flamelet-based approaches involving pre-tabulation have been successfully applied to a variety of combustion applications[2]-[3]. The original method employed look-up tables based on mixture fraction and its variance but is well known to be inadequate for simulating topologically complex flames. [4]-[6]. For example, mixture fraction alone is insufficient to model the full physical complexity

of lifted flames. It has been shown that the use of a progress variable in addition to the mixture fraction is required to capture the complex physics of these flames in a computationally tractable manner – the flamelet progress variable (FPV) approach has been shown to better capture the complex physics in detached flames [7]-[8]. A flamelet progress model (FPV) has previously been implemented in Loci-STREAM [9]-[10] and has been used for a variety of rocket engine combustion simulations at NASA [11]-[14]. The original flamelet approach was developed in the context of gas-gas combustion for which assumptions of low-Mach number and ideal gas thermodynamics are valid. In the context of liquid rocket combustion, the FPV model has been successfully extended for supercritical simulations. However, the extension of the classical FPV model to trans- and supercritical flow simulations in the fully compressible context, specifically with regards to the pressure and temperature coupling, has not been widely reported. A relatively recent development in this regard is the compressible flamelet model proposed by Ma et al. [15] who developed such a model in the context of a fully explicit finite volume solver. The solution of the laminar flamelets in mixture fraction space and the chemistry tabulation requires special considerations in order to fully model the non-linear effects in transcritical flows. A similar approach is adopted here. Moreover, this approach is developed here as a fully compressible combustion model in the context of a fully implicit all-speed solver, i.e., Loci-STREAM.

The fully compressible flamelet progress variable model (CFPV) presented here employs the classical flamelet methodology as the foundation and extends it to account for compressibility involving both ideal and real fluids. The ideal-gas thermodynamics is modeled by linearizing the specific heat ratio and the cubic Peng-Robison equation of state (PR EoS) is employed to account for real-fluid effects. The parameters needed for the PR EoS are pre-tabulated for the evaluation of departure functions and a quadratic expression (as a function of temperature) is used to model the attraction parameter. This compressible flamelet model is able to account for temperature and pressure variations from the baseline flamelet table in a computationally tractable manner. Unlike standard flamelet models, this compressible flamelet capability seamlessly handles all parts of the combustion domain, including the upstream fuel and oxidizer manifold sections, the combustion chamber and the highly compressible nozzle.

2 Methodology

2.1 The Programming Framework – Loci

The framework used for the development of Loci-STREAM is called Loci [16] which is a programming environment designed to reduce the complexity of assembling large-scale finite-volume applications as well as the integration of multiple applications in a multidisciplinary environment. This allows: (a) a seamless integration of multidisciplinary physics in a unified manner, and (b) an automatic handling of massively parallel computing. Unlike traditional procedural programming systems (C, FORTRAN) in which one writes code with subroutines, or object-oriented systems (C++, Java) in which objects are the major program components, Loci uses a rule-based framework for application design. Users of Loci write applications using a collection of "rules" and provide an implementation for each of the rules in the form of a C++ class. In addition, the user must create a database of "facts" which describe the particular knowns of the problem, such as boundary conditions. Once the rules and facts are provided, a query is made to have the system construct a solution. One of the powerful features of Loci is its ability to automatically determine the scheduling of events of the program to produce the answer to the desired query, as well as to test the consistency of the input to determine whether a solution is possible given the specified information. The other major advantage of Loci to the application developer is its automatic handling of domain decomposition and distribution of the problem to multiple processors.

2.2 Numerical Algorithm

The computational tool, Loci-STREAM, is a parallel CFD solver. Its versatility lies in an all-speed methodology which allows a seamless computation of flows involving a wide range of Mach numbers, i.e., incompressible to hypersonic in a unified manner. It can be used for a wide variety of applications

involving multiphase, compressible/incompressible, laminar/turbulent flows, with or without chemical reactions and phase change. For handling complex geometries, it allows generalized unstructured grids with arbitrary polyhedral cells. Loci-STREAM integrates proven numerical methods for generalized grids and state-of-the-art physical models – the methodologies embedded in Loci-STREAM enable routine simulations of unsteady flows in complex geometries such as liquid rocket engines requiring large unstructured grids and complex multidisciplinary physics [9]-[10].

The Loci-STREAM flow solver is based on the SIMPLE (Semi-Implicit Method for Pressure-Linked Equations) algorithm [17] and its variants, SIMPLEC and PIMPLE algorithms. It uses a control volume approach with a collocated arrangement for the velocity components and the scalar variables. In the standard algorithm, the so-called momentum interpolation approach [18] is employed to prevent pressure-velocity decoupling which involves adding a fourth-order pressure dissipation term while estimating the mass flux at the control volume interfaces. The velocity components are computed from the respective momentum equations. The velocity and the pressure fields are corrected using a pressure correction equation. The correction procedure leads to a continuity-satisfying velocity field. The whole process is repeated until the desired convergence level is reached.

The spatial discretization options employed in Loci-STREAM include the standard second-order central differencing for the viscous fluxes and the standard first-order upwind (FOU), second-order upwind (SOU) and central difference (CD) schemes for the convective fluxes [19]. In order to accurately compute flows involving all-speed flow regimes – from nearly incompressible to highly compressible flow regions within the same computational domain (such as in the entire flow path of a liquid rocket injector), robust and accurate numerical schemes capable of seamlessly handling a wide range of Mach numbers are also implemented in Loci-STREAM. These include compressible, characteristic based convection schemes such as AUSM+[20], SLAU[21] and SLAU2[22]– these schemes are robust in the high-speed as well as the low-speed regions of the flow field, thus allowing these schemes to be used in an all-speed manner. Time-stepping schemes implemented in Loci-STREAM include the first-order backward difference (BDF) scheme, the second-order backward difference (BDF2) scheme and the second-order Crank-Nicholson (CN) scheme.

The basic governing equations used are the Favre-averaged Navier-Stokes equations, as given below:

$$\frac{\partial \bar{\rho}}{\partial t} + \frac{\partial \bar{\rho} u_j}{\partial x_j} = 0 \tag{1}$$

$$\frac{\partial \bar{\rho} u_i}{\partial t} + \frac{\partial \bar{\rho} u_j u_i}{\partial x_j} = -\frac{\partial \bar{p}}{\partial x_i} + \frac{\partial}{\partial x_j}\left(\tilde{\tau}_{ij} - \overline{\rho u_i'' u_j''}\right) \tag{2}$$

$$\begin{aligned}\frac{\partial \bar{\rho} E}{\partial t} + \frac{\partial}{\partial x_j}\left(\bar{\rho} u_j E\right) = \frac{\partial}{\partial x_j}\left[\left(\frac{\lambda}{c_p} + \frac{\mu_t}{Pr_t}\right)\frac{\partial h}{\partial x_j}\right] + \frac{\partial}{\partial x_j}\left(\sum_{k=1}^{NS}\left(\bar{\rho} D_k - \frac{\lambda}{c_p}\right) h_k \frac{\partial Y_k}{\partial x_j}\right) + \\ \frac{\partial}{\partial x_j}\left[u_j\left(\tilde{\tau}_{ij} - \overline{\rho u_i'' u_j''}\right) - u_j p\right]\end{aligned} \tag{3}$$

where

$$\tilde{\tau}_{ij} = \mu\left(\frac{\partial u_i}{\partial x_j} + \frac{\partial u_j}{\partial x_i}\right) - \frac{2}{3}\mu\frac{\partial u_k}{\partial x_k}\delta_{ij} \tag{4}$$

$$-\overline{\rho u_i'' u_j''} = \mu_t\left(\frac{\partial u_i}{\partial x_j} + \frac{\partial u_j}{\partial x_i}\right) - \frac{2}{3}\mu_t\frac{\partial u_k}{\partial x_k}\delta_{ij} - \frac{2}{3}\bar{\rho} k \delta_{ij} \tag{5}$$

In the above, ρ is the density of the mixture, u_i is the i^{th} component of the velocity vector, p is the pressure, E is the total energy including the chemical energy, h_i, is the species enthalpy and Y_i the

species mass fraction. μ and μ_t are the laminar viscosity and eddy viscosity, respectively. C_p is the specific heat, λ is the thermal conductivity, τ_{ij} are the viscous stresses, D is the species diffusivity and Pr_t is the turbulent Prandtl number. The system is closed with the Peng-Robinson equation of state (PR EoS) which is discussed later. The flamelet-based combustion model is also discussed later.

For turbulence closure, a hierarchy of models is implemented in Loci-STREAM. The Reynolds-Averaged Navier-Stokes (RANS) models include variants of the k-ε model [23], k-ω model [24] and Menter's SST model [25]. Large Eddy Simulation (LES) models include the Smagorinsky model [26] and the WALE model [27]. Hybrid-RANS-LES models include Detached-Eddy Simulation (DES) [28] and its variants, DDES and IDDES [29] as well as the Nelson-Nichols model [30].

2.3 Flamelet Models

Accounting for the coupling between turbulence and the chemical reactions is one of the challenges in turbulent combustion modeling. An attractive approach in terms of computational cost is to reduce the dimensionality of the problem by utilizing the concept of conserved scalars [31]. The statistics of the conserved scalar are described with a presumed shape PDF. The problem is then transformed to one of linking the conserved scalar to the reactive scalars such as species mass fractions and temperature. This step is often associated with assumptions regarding the flame structure and chemistry speed and/or complexity.

Conserved scalars are quantities that are unchanged by the chemical reactions. A normalized conserved scalar called the mixture fraction (Z) can be defined such that it takes the value of 0 in the oxidizer stream and 1 in the fuel stream. Depending on the combustion regime, the mixture fraction along with other suitable variables can be used to describe the flame structure allowing a reduction in the dimensionality of the problem. Consider Figure 1 which shows the generic response of the heat release by a one-dimensional laminar diffusion flame in the form of the so-called S-shaped curve. Figure 1(a) shows the heat release versus the Damkohler number (Da) whereas Figure 1(b) shows the corresponding variation of stoichiometric temperature with the stoichiometric scalar dissipation rate. Note that the stoichiometric scalar dissipation rate is related to the Damkohler number. The upper branch of the S-shaped curve represents the combusting regime. Starting from the upper branch, if the diffusion time scale is decreased (e.g., by increasing flow rates), the Da reduces and the heat generated by reactions are diffused from the reaction zone faster until the reactions cannot keep up and the quenching limit is reached. After quenching, a regime of pure mixing without combustion, represented by the lower branch of the curve, is attained. Starting from the lower branch, however, when the Da is increased, the same path is not followed. Instead, the pure mixing regime exists until the ignition Da is reached. After ignition, a rapid transition to the upper branch follows. Referring to Figure 1, if the

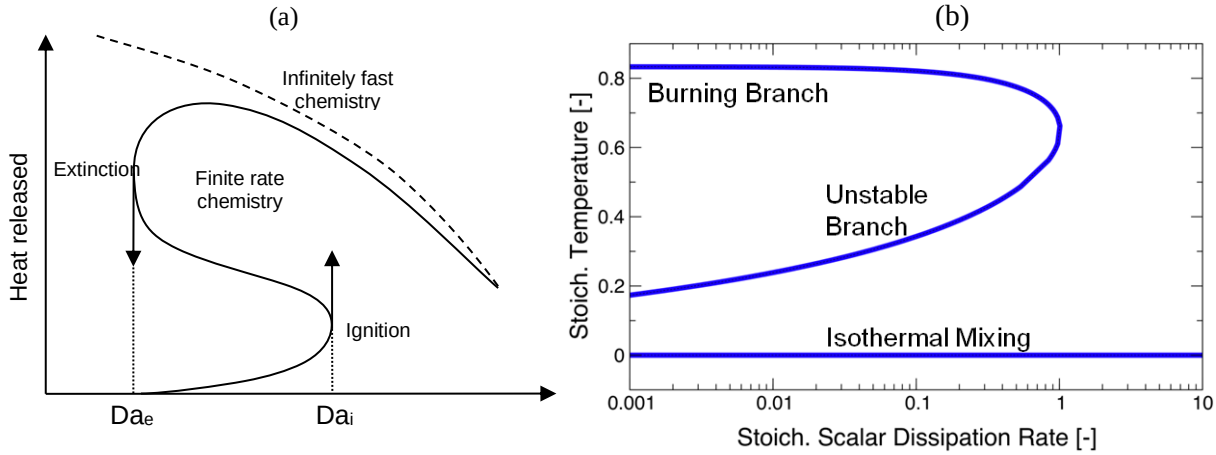

Figure 1. *Generic response of the heat released by a 1-dimensional laminar diffusion flame. (a) Heat release vs, Damkohler number; (b) Stoichiometric temperature vs. scalar dissipation rate.*

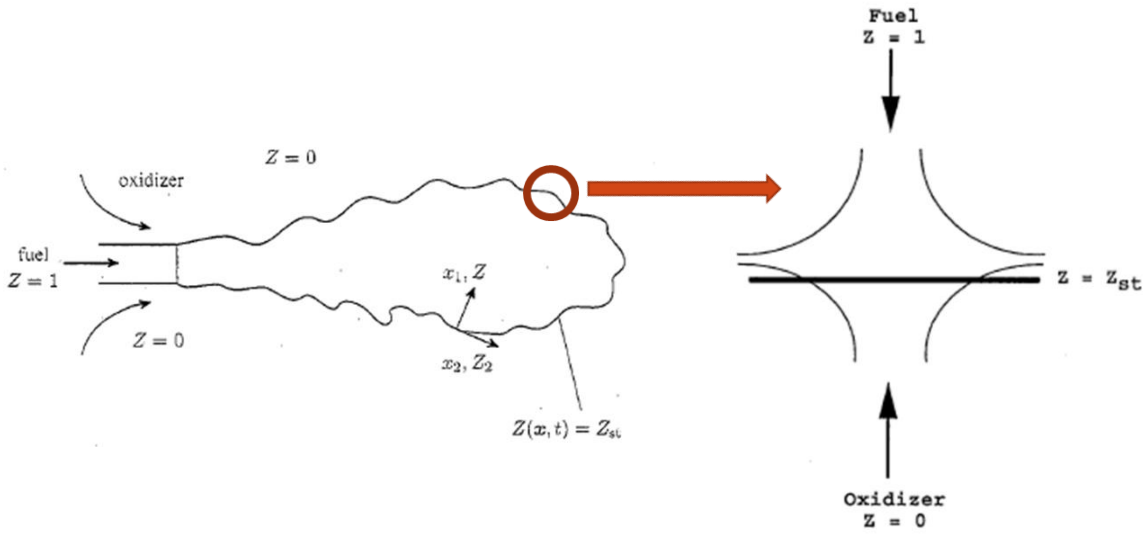

Figure 2. *Flamelet model concept.*

chemistry were assumed to be infinitely fast in the analysis of such a flame, flame stretching would not be captured. The infinitely fast chemistry approach corresponds to the dashed line in Figure 1(a) for which the flame is completely described with the knowledge of mixing and hence the mixture fraction variable distribution alone is sufficient to describe the flame.

If the flame is described by the mixture fraction variable (Z) as well as the scalar dissipation rate (χ), finite-rate chemistry effects can be recovered. However, whether the flame is extinguished or ignited, corresponding to the lower or the upper branches of the solid curve in Figure 1(a), respectively, depends on the path followed, as discussed above. A third quantity is then needed to fully determine the regime. A quantity called the progress variable is often employed in the context of extensions to the basic flamelet model.

Flamelet-based approaches involving pre-tabulation have been successfully applied to a variety of combustion applications [2]-[3]. The original method employing look-up tables based on mixture fraction and its variance has proven to be inadequate for simulating topologically complex flames [4]-[6]. For example, mixture fraction alone is insufficient to model the full physical complexity of lifted flames. It has been shown that the use of a progress variable in addition to the mixture fraction is required to capture the complex physics of these flames in a computationally tractable manner – the flamelet progress variable (FPV) approach has been shown to better capture the complex physics in detached flames [7]-[8]. In the context of liquid rocket combustion, the FPV approach has been used for supercritical simulations. The extension of the FPV model for transcritical and supercritical flows in the fully compressible context – specifically with regards to the pressure and temperature coupling – in a fully implicit all-speed CFD solver is the main objective of the present work.

2.3.1 Steady Flamelet (SF) Model

Flamelet models are based on the view of a turbulent diffusion flame as an ensemble of stretched laminar flamelets (see Figure 2). Inherent to this view is the assumption of a thin reaction zone which is thinner than the scale of a Kolmogorov eddy. The effect of turbulence is therefore limited to the deformation and stretching of the flame sheet but does not penetrate the reaction zone. Flamelets can then be viewed as thin laminar reactive diffusive layers embedded in an otherwise non-reacting turbulent flow field. The local reactive-diffusive balance in flamelets are viewed as similar to that of a laminar flame with the same mixture fraction (Z) and scalar dissipation rate (χ).

Flamelet equations are derived via a Crocco-type coordinate transformation of the species mass fraction and energy equations. The original coordinate system is selected such that the x_2 and x_3 are locally aligned to the flame surface which is determined by the stoichiometric mixture fraction, $Z = Z_{st}$. Then x_1, which is normal to the stoichiometric surface, is replaced by Z. The transformation, as illustrated in Figure 2, can be represented as:

$$(t, x_1, x_2, x_3) \rightarrow (\tau, Z, Z_1, Z_2) \tag{6}$$

where $\tau = t$, $Z = x_1$, $Z_2 = x_2$ and $Z_3 = x_3$. The laminar flamelet model utilizes the conserved-scalar approach in which all thermo-chemical quantities (such as the species mass fractions and temperature) are represented in terms of a reduced number of scales, namely the mixture fraction, Z, and the scalar dissipation rate, χ. These thermo-chemical quantities are obtained from the solution of the steady laminar flamelet equations which are the species and energy equations transformed in the mixture fraction space; these equations can be written as the following:

$$\rho \frac{\partial Y_i}{\partial \tau} = \rho \frac{\chi}{2} \frac{\partial^2 Y_i}{\partial Z^2} + \dot{\omega}_i \tag{7}$$

$$\rho \frac{\partial T}{\partial \tau} = \rho \frac{\chi}{2} \frac{\partial^2 T}{\partial Z^2} - \sum_{i=1}^{NS} \frac{h_i}{C_p} \dot{\omega}_i + \frac{1}{C_p} \frac{\partial p}{\partial \tau} \tag{8}$$

where T is the temperature, $\dot{\omega}_i$ is the species production rate and χ is the scalar dissipation rate.

In Eqs. (7) and (8), the scalar dissipation rate appears as an external parameter. Pitsch et al. [3] considered a semi-infinite mixing layer to obtain the following analytical expression:

$$\chi(Z) = \chi_{st} \frac{Z^2}{Z_{st}^2} \frac{\ln(Z)}{\ln(Z_{st})} \tag{9}$$

In space propulsion systems, fuel conversion and chemical reactions occur on time scales that are typically significantly shorter compared to the characteristic kinematic scales that are associated with turbulence and hydrodynamics. In these large-Damkohler number flows, all thermochemical quantities are in a steady state. As a consequence, transient effects in Eqs. (7) and (8) become negligible, so that the species and temperature distributions can accurately be presented by the solution of the steady flamelet equations. In this context, it is important to point out that, although transient effects in the flamelet equations are neglected, the dynamics of the combustion processes and the interaction between turbulence and reaction chemistry is fully accounted for; the only limitation that arises from such a steady flamelet modeling approach is that chemical effects that evolve on relatively slower temporal scales compared to the characteristic hydrodynamics scales (such as during auto-ignition or slow nitric-oxide pollutant formation), are not accurately represented.

Using Eq. (9), the flamelet equations (7) and (8) can be parameterized by only χ. All thermochemical quantities, $\psi = \{Y_i, T\}$, are then parameterized in the following functional form:

$$\psi = f(Z, \chi) \tag{10}$$

Using a specified reaction mechanism, Eq. (10) can be tabulated into a library (table) as a preprocessing step for turbulent combustion computations. The above approach is referred to as the Steady Flamelet (SF) model.

In order to account for the turbulence-chemistry interaction for the prediction of turbulent reacting flows, the state relation (10) must be formulated for Favre-averaged or Favre-filtered quantities. The Favre-averaged or Favre-averaged thermochemical quantities are computed from Eq. (10) by employing a presumed shape joint PDF for the mixture fraction and the scalar dissipation rate. Thus, the flamelet results are convoluted with a joint PDF, as follows:

$$\tilde{\psi} = \int_Z \int_\chi \psi \, \tilde{P}(Z, \chi) \, d\chi \, dZ \tag{11}$$

The mixture fraction and the scalar dissipation are are assumed to be uncorrelated, and Eq. (11) can be written as

$$\tilde{\psi} = \int_Z \int_\chi \psi \, \tilde{P}(Z) \, P(\chi) \, d\chi \, dZ \tag{12}$$

A beta PDF is used for the convolution of Z which is parameterized in terms of the first two moments of Z; its two parameters can be related to the first two moments of Z as follows:

$$P(Z) = \frac{Z^{\alpha-1}(1-Z)^{\beta-1}}{\int_0^1 Z^{\alpha-1}(1-Z)^{\beta-1} \, dZ} \tag{13}$$

where

$$\alpha = Z\left[\frac{Z(1-Z)}{Z''^2} - 1\right] \tag{14}$$

$$\beta = (1-Z)\left[\frac{Z(1-Z)}{Z''^2} - 1\right] \tag{15}$$

For $\tilde{P}(\chi)$, a lognormal distribution is assumed. This assumption has been tested and verified by several authors. The lognormal distribution for the scalar dissipation rate is given as:

$$P(\chi_{st}) = \frac{1}{\chi_{st}\sigma\sqrt{2\pi}} \exp\left\{-\frac{1}{2\sigma^2}(\ln\chi_{st} - \mu)^2\right\} \tag{16}$$

with

$$\begin{aligned} \chi_{st} &= \exp\left(\mu + \frac{1}{2}\sigma^2\right) \\ \chi_{st}''^2 &= \chi_{st}^2\left(\exp\sigma^2 - 1\right) \end{aligned} \tag{17}$$

The PDF of the scalar dissipation rate is known if the σ and χ_{st} are given. σ is assumed to be unity whereas χ_{st} is obtained using Eq. (21) given below. The PDFs are constructed so as to reproduce Z, Z''^2 and χ_{st}. As a result, the mean composition of the mixture can be obtained with the knowledge of these three quantities. Flamelet equations can be pre-solved for a number of Z and χ values and the results can be integrated through the PDFs constructed for a range of $\tilde{Z}, \widetilde{Z''^2}$ and $\tilde{\chi}_{Z,st}$ values, enabling a tabulation which can be represented as

$$Z,\ Z''^2,\ \chi_{Z,st} \xrightarrow{\text{PDF table lookup}} \tilde{\psi} \equiv \left\{\tilde{Y}_i,\ \tilde{T}\right\} \tag{18}$$

The beta PDF model requires the solution of the following additional transport equations (in the CFD solver) for the mean and variance of the mixture fraction:

$$\frac{\partial \bar{\rho} Z}{\partial t} + \frac{\partial \bar{\rho} u_j Z}{\partial x_j} = \frac{\partial}{\partial x_j}\left[\left(\bar{\rho} D + \frac{\mu_t}{Sc_t}\right)\frac{\partial Z}{\partial x_j}\right] \tag{19}$$

$$\frac{\partial \bar{\rho} Z''^2}{\partial t} + \frac{\partial \bar{\rho} u_j Z''^2}{\partial x_j} = \frac{\partial}{\partial x_j}\left(\frac{\mu_t}{Sc_t}\frac{\partial Z''^2}{\partial x_j}\right) + 2\frac{\mu_t}{Sc_t}\frac{\partial Z''^2}{\partial x_j}\frac{\partial Z''^2}{\partial x_j} - \bar{\rho}\chi \tag{20}$$

where D is the diffusion coefficient for the mixture fraction and Sc_t is the Schmidt number. The mean scalar dissipation rate is obtained from an algebraic model:

$$\chi = c_\chi c_\mu \omega Z''^2, \quad \text{where } c_\chi = 2,\ c_\mu = 0.09 \tag{21}$$

To summarize, the underlying assumption of the flamelet model is that the turbulent flame consists of an ensemble of laminar stretched by the surrounding turbulent flow structure. Solutions for such flamelets, typically modeled as a counter diffusion flow problem, are pre-computed and parameterized

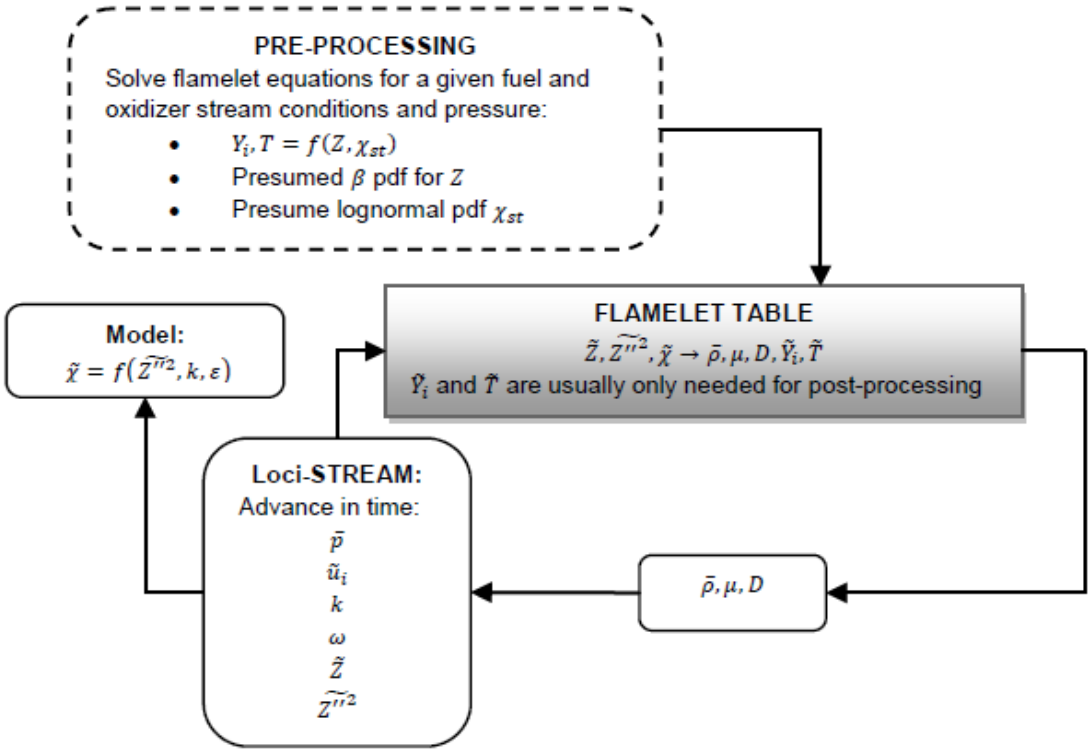

Figure 3. *Flow chart for coupling the flamelet model with Loci-STREAM.*

with the scalar dissipation rate. The resulting flamelets are mapped from the Z field into the laminar mixture composition field for each scalar dissipation rate. These are further processed by convoluting with presumed shape probability density functions (PDFs) to represent turbulent statistics. Finally, the results are tabulated as a three-dimensional lookup table as follows:

$$Z, Z''^2, \chi \rightarrow \bar{\rho}, \tilde{\mu}, D, Y_i, T \tag{22}$$

The coupling of the flamelet model with the CFD solver (Loci-STREAM) is illustrated in Figure 3.

It should be noted that when χ approaches zero, the flamelet model becomes equivalent to the presumed PDF/equilibrium model. The latter is simpler and more convenient when non-equilibrium effects are negligible. In the PDF/equilibrium model, the equilibrium state for a given mixture fraction value can be uniquely determined from the mixture fraction variable and the minimization of Gibb's free energy. Turbulent statistics of the mixture fraction can still be represented via the presumed shape PDFs.

2.3.2 Flamelet Progress Variable (FPV) Model

A major limitation of the steady flamelet (SF) model arises from the parameterization of the thermochemical quantities, in which mixture fraction Z and scalar dissipation rate $\chi_{Z,st}$ are used. In particular, this parameterization of the entire flamelet solution space is not unique and results in multiple solutions for $\chi_{Z,i} \leq \chi_{Z,st} \leq \chi_{Z,q}$ where "i" represents auto-ignition and "q" represents flame quenching or extinction (see Figure 4(a)). This can be seen in Figure 4(b) which shows that three flamelet solutions (temperature profiles) are possible – corresponding to the three branches of the S-shaped curve – for the same scalar dissipation rate of $\chi_{Z,st}$=1 s^{-1} (given by the location of the dashed vertical line in Figure 4(a)). In the SF model, in order to obtain a unique solution, the upper (burning) branch is always chosen, thus excluding any possibility of unsteady effects such as auto-ignition or local flame quenching. To overcome this limitation, a flamelet/progress variable (FPV) formulation has been developed[7]-[8]. In the FPV model, a reaction progress variable C is introduced as a parameter, which replaces the scalar dissipation rate. This progress variable (C) represents the progress of the reaction locally and is defined

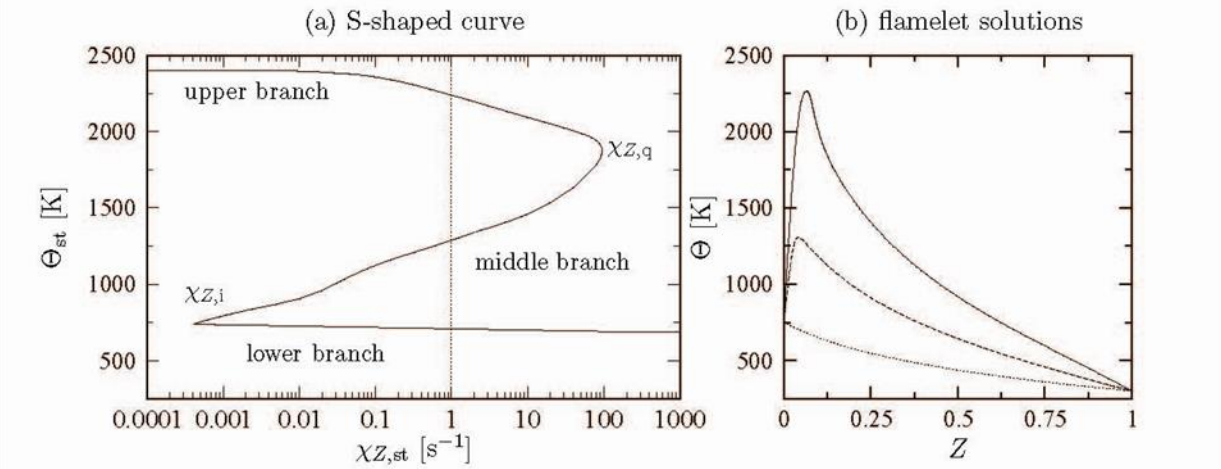

Figure 4. *S-shaped curve illustrating multiple solutions resulting from steady flamelet (SF) model.*

using a linear combination of reaction product species. As an example, for methane/air chemistry the following definition is commonly used:

$$C = Y_{CO_2} + Y_{H_2O} + Y_{H_2} + Y_{CO} \tag{23}$$

Such a specification allows a unique identification of each single flamelet along the entire S-shape curve. This effectively means that, compared to the SF model, the FPV model employs a horizontal projection onto the S-shaped curve, as shown in Figure 5, so that a unique flamelet solution is always obtained along the S-shaped curve.

In the FPV model, transport equations for the mixture fraction (Z) and the progress variable (C) are solved. The transport equation for Z is given by Eq. (19) and the transport equation for C is given by the following:

$$\frac{\partial \rho C}{\partial t} + \frac{\partial \rho u_j C}{\partial x_j} = \frac{\partial}{\partial x_j}\left(\rho\alpha \frac{\partial C}{\partial x_j}\right) + \rho\dot{\omega}_C \tag{24}$$

where $\dot{\omega}_C$ is the production rate for the progress variable.

All thermochemical quantities are parameterized in terms of mixture fraction Z and progress variable C, and the turbulence/chemistry interaction is modeled through a presumed PDF closure model. The parameterization can be represented as:

$$Z,\ Z''^2, C \xrightarrow{\text{PDF table lookup}} \tilde{Y}_i,\ \tilde{T} \tag{25}$$

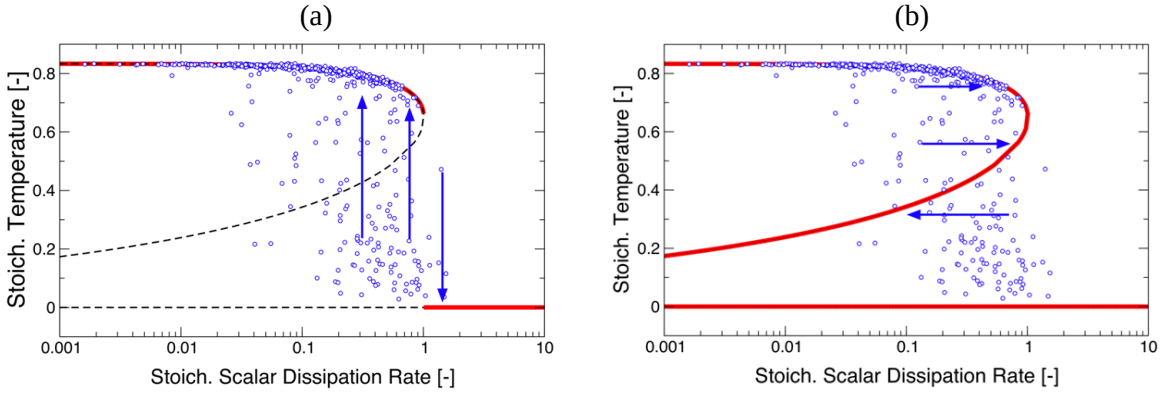

Figure 5. *Comparison of the Steady Flamelet (SF) Model and the Flamelet/Progress variable (FPV) model: (a) the horizontal projection used in the SF model and (b) the vertical projection used in the FPV model. The solid (red) lines show the accessible solution in the SF (a) and the FPV (b) models.*

To summarize, in the Flamelet/Progress Variable (FPV) approach, the chemistry is precomputed and tabulated as a series of laminar flamelet solutions. Flamelets are first computed for different values of the scalar dissipation rate at a constant background pressure and specified constant fuel and air temperatures, and then the flamelets are parametrized by the mixture fraction and the reaction progress variable. The resulting flamelet table is used for the determination of the local temperature, species, density, source term of the progress variable and other thermal-transport quantities needed by the CFD solver. Presumed PDFs are introduced to account for the turbulence/chemistry interaction. Typically, a beta-PDF is used for the mixture fraction and a delta-PDF for the progress variable, which has been shown to be a reasonable approximation in many studies. Since the reacting region is typically in the ideal gas regime even under transcritical combustion conditions, the PDF closures perform similarly as for ideal gas reacting flows.

2.4.3 Thickened Flame Model

An alternative turbulence-chemistry closure called the Thickened Flame (TF) model is also commonly employed [41]-[43]. The basic idea of the Thickened Flame model is to move the turbulence closure for the chemical source terms out of the flamelet tables, bringing it instead into the governing PDEs being solved by the CFD solver. The concepts underlying thickened flame closure evolved from the analytical investigation of the fundamental conservation equations governing laminar premixed flames as well as the DNS solution of such flames [41]. In general, when numerically simulating the propagation of a premixed flame on a grid of finite resolution, an adequate resolution of the flame is required to avoid numerical difficulties. Resolving the flame implies that the flame thickness must be captured over multiple cells in the grid. Generally, however, an actual flame is much thinner than the minimum cell size in the mesh. From basic analytical work [41] it was found that if the molecular diffusivities in the governing equations are multiplied by a flame thickening factor, F, and at the same time the reaction rates in the governing equations are divided by the same factor, an equivalent thickened flame will result. This flame will be F times thicker than the original flame (and able to be resolved on the mesh) but will have the same flame speed as the original flame. Subsequent research [42], however, found that the resulting thickened flame did not respond in the same manner as the original flame to eddies in the flow field. Typically, a flame exposed to swirling eddies in the flow will stretch and fold (or wrinkle). As a result of this, the surface area of the flame front separating unburned fuel and oxidizer is increased, leading generally to an increased net reaction rate and thus an increased heat release per unit volume around the flame front. In order to counter the reduction in stretching and wrinkling of the thickened flame compared to the original flame, a so-called efficiency function, E, was introduced into the formulation which effectively enhances the reaction rate term in the governing equations. The resulting governing equations for mixture fraction and progress variable in the flamelet formulation, when using thickened flame closure, appear as follows, where multiplicative factors due to the closure model appear in the diffusion terms:

$$\frac{\partial \bar{\rho} Z}{\partial t} + \frac{\partial \bar{\rho} u_j Z}{\partial x_j} = \frac{\partial}{\partial x_j}\left[\left(\bar{\rho} D(EF) + \frac{\mu_t}{Sc_t}\right)\frac{\partial Z}{\partial x_j}\right] \tag{26}$$

$$\frac{\partial \bar{\rho} C}{\partial t} + \frac{\partial \bar{\rho} \tilde{u}_j C}{\partial x_j} = \frac{\partial}{\partial x_j}\left(\bar{\rho} D(EF)\frac{\partial C}{\partial x_j}\right) + \bar{\rho}\dot{\omega}_C\left(\frac{E}{F}\right) \tag{27}$$

In the original thickened flame closure model (Colin et al [42]), the flame thickening factor was specified as a constant value in the range $5<F<30$. The efficiency function, E, on the other hand was determined on a point-by-point basis in the flow using a rather complex procedure designed to quantify the local flame wrinkling due to resolved and unresolved (sub-grid) flow motions and its effective increase in the local heat release. Vreman et al [43] designed a new variation of the thickened flame closure approach which is substantially easier to implement and is more amenable to be employed with a variety of turbulence models (RANS, DES, LES). Noting that the multiplicative factor EF which multiplies the molecular diffusivity in Eqs. (26) and (27) can be tied to the underlying turbulence model (giving a spatially-varying thickening of the flame), this product is given by the following relation:

$$F^{1+\alpha} = EF = \frac{D + \mu_t / \left(\bar{\rho} Sc_t \right) + D_n}{D} \tag{28}$$

One can see that the product *EF* is essentially the ratio of the total diffusion to the molecular diffusion. Strictly speaking, this total diffusion includes the original laminar diffusion (*D*), the turbulent diffusion arising from the use of a turbulence model (μ_t is the eddy viscosity resulting from the turbulence model and Sc_t is the turbulent Schmidt number) as well as the diffusion (D_n) arising from the numerical treatment of the convection term in the governing equations (this last term is commonly neglected). As a result of this definition of *EF*, in actuality, no modification of the existing diffusion terms in Loci-STREAM need be made since the existing turbulent diffusion coefficient is exactly the product $D \times EF$ (referring to the equations above). One needs simply to be able to compute the factor (E/F) which then multiplies the chemical source terms. To this end, Vreman et al [43] proposed a simple model which relates the efficiency function *E* to the flame thickening factor as

$$E = F^{\alpha}, \quad 0 < \alpha < 2/3 \tag{29}$$

where the theoretical limits of α were originally established by Colin et al [42]. Using this relation, the final expression for the factor (E/F) which multiplies the chemical source term in the governing equations of Loci-STREAM assumes the following form:

$$\frac{E}{F} = \left(F \right)^{\alpha - 1} \tag{30}$$

Increasing the effective viscosity results in more damping of the chemical source term, whereas increasing flame wrinkling efficiency results in less damping of the chemical source term. For RANS simulations, in which the flame may be several cells thick, local damping factors can range anywhere from $0.1 < (E/F) < 0.5$. For DES and LES simulations in which the viscosity ratios are much lower, damping factor will generally fall in the range $0.8 < (E/F) < 0.95$. Reversion to proper DNS behavior is satisfied in the sense that as the eddy viscosity approaches zero, resulting in a viscosity ratio of unity, the damping factor (E/F) also approaches unity, implying no modification of the laminar reaction source term values.

2.5 Compressible FPV (CFPV) Model for Super- and Trans-Critical Flows

An extension of the classical FPV approach has been proposed for trans- and supercritical combustion simulations in the context of finite volume, fully compressible, fully explicit solvers by Ma et al [15]. The solution of the laminar flamelets in mixture fraction space and the chemistry tabulation requires special considerations in order to fully model the non-linear effects in transcritical flows. A similar approach is adopted here. Moreover, this approach is developed here as a fully compressible combustion model in the context of a fully implicit all-speed solver, i.e., Loci-STREAM.

The approach presented in this section utilizes the flamelet (FPV) methodology extended to account for compressibility involving both ideal and real fluids. The ideal-gas thermodynamics is modeled by linearizing the specific heat ratio whereas the parameters needed for the cubic Peng Robinson equation of state are pre-tabulated for the evaluation of departure functions and a quadratic expression is used to model the attraction parameter. This compressible model is able to account for temperature and pressure variations from the baseline flamelet table using a computationally tractable pre-tabulated combustion chemistry in a thermodynamically consistent fashion.

2.5.1 Thermodynamic Properties Using Peng-Robinson EoS

In the compressible combustion model of the present work, augmenting the governing PDEs presented in Section 2.2 is a flamelet tabulation procedure which is based on the Peng-Robinson equation of state (PR-EoS) that provides both ideal-gas reference state and real-fluid thermodynamic information about the mixture (for a given Z and C). The Peng-Robinson (PR) equation of state [34] is employed for the evaluation of thermodynamic quantities; it can be written as:

$$p = \frac{RT}{v-b} - \frac{a}{v^2 + 2bv - b^2} \tag{31}$$

where p is the pressure, R is the gas constant, T is the temperature, v is the specific volume, and the attraction parameter a and the effective molecular volume b are dependent on temperature and composition to account for effects of intermolecular forces. For mixtures, the parameters a and b are evaluated as follows:

$$a = \sum_{\alpha=1}^{N_s} \sum_{\beta=1}^{N_s} X_\alpha X_\beta a_{\alpha\beta} \tag{32}$$

$$b = \sum_{\alpha=1}^{N_s} X_\alpha b_\alpha \tag{33}$$

where X_α is the mole fraction of species α. Extended corresponding states principle and single-fluid assumption for mixtures are adopted [35]-[36]. The parameters a and b are evaluated using the mixing rules recommended by Harstad et al. [37]:

$$a_{\alpha\beta} = 0.457236 \frac{\left(RT_{c,\alpha\beta}\right)^2}{p_{c,\alpha\beta}} \left(1 + c_{\alpha\beta}\left(1 - \sqrt{\frac{T}{T_{c,\alpha\beta}}}\right)\right)^2 \tag{34}$$

$$b_\alpha = 0.077796 \frac{RT_{c,\alpha}}{p_{c,\alpha}} \tag{35}$$

$$c_{\alpha\beta} = 0.37464 + 1.54226\omega_{\alpha\beta} - 0.26992\omega_{\alpha\beta}^2 \tag{36}$$

where $T_{c,\alpha}$ and $p_{c,\alpha}$ are the critical temperature and pressure of species α, respectively. The critical mixture conditions for temperature $T_{c,\alpha\beta}$, pressure $p_{c,\alpha\beta}$ and acentric factor $\omega_{c,\alpha\beta}$ are determined using the corresponding state principles [38].

Partial derivatives and thermodynamic quantities based on PR-EoS that are required for evaluating other thermodynamic variables can be derived analytically, as given below:

$$\left(\frac{\partial p}{\partial T}\right)_{v,X_i} = \frac{R}{v-b} - \frac{\left(\partial a/\partial T\right)_{X_i}}{v^2 + 2bv - b^2} \tag{37}$$

$$\left(\frac{\partial p}{\partial T}\right)_{\mathrm{T},X_i} = -\frac{RT}{\left(v-b\right)^2} \left\{1 - 2a\left[RT\left(v+b\right)\left(\frac{v^2+2bv-b^2}{v^2-b^2}\right)^2\right]^{-1}\right\} \tag{38}$$

$$\left(\frac{\partial a}{\partial T}\right)_{X_i} = -\frac{1}{T} \sum_{\alpha=1}^{N_s} \sum_{\beta=1}^{N_s} X_\alpha X_\beta a_{\alpha\beta} G_{\alpha\beta} \tag{39}$$

$$\left(\frac{\partial^2 a}{\partial T^2}\right)_{X_i} = 0.457236 \frac{R^2}{2T} \sum_{\alpha=1}^{N_s} \sum_{\beta=1}^{N_s} X_\alpha X_\beta c_{\alpha\beta}\left(1 + c_{\alpha\beta}\right) \frac{T_{c,\alpha\beta}}{p_{c,\alpha\beta}} \sqrt{\frac{T_{c,\alpha\beta}}{T}} \tag{40}$$

$$G_{\alpha\beta} = \frac{c_{\alpha\beta}\sqrt{T/T_{c,\alpha\beta}}}{1 + c_{\alpha\beta}\left(1 - \sqrt{T/T_{c,\alpha\beta}}\right)} \tag{41}$$

$$K_1 = \int_{+\infty}^{v} \frac{dv}{v^2 + 2bv - b^2} = \frac{1}{\sqrt{8b}} \ln\left(\frac{v + (1-\sqrt{2})/b}{v + (1+\sqrt{2})/b} \right) \tag{42}$$

For real fluids, thermodynamic quantities are typically evaluated from the ideal-gas value plus a departure function that accounts for the deviation from the ideal-gas behavior. The ideal-gas enthalpy, entropy and specific heat are evaluated from the NASA polynomials at a reference temperature of 298 K. The specific internal energy can be written as

$$e(T, \rho, X_i) = e^{ig}(T, X_i) + \int_0^{\rho} \left[p - T\left(\frac{\partial p}{\partial T} \right)_{\rho, X_i} \right] \frac{d\rho}{\rho^2} \tag{43}$$

where the superscript "*ig*" indicates the ideal-gas value of the thermodynamic quantity, and the above can be integrated analytically for PR-EoS to give

$$e = e^{ig} + K_1 \left[a - T\left(\frac{\partial a}{\partial T} \right)_{X_i} \right] \tag{44}$$

where K_1 is evaluated using Eq. (42). The specific enthalpy can be expressed as:

$$h = h^{ig} - RT + K_1 \left[a - T\left(\frac{\partial a}{\partial T} \right)_{X_i} \right] + pv \tag{45}$$

The specific heat capacity at constant volume and constant pressure, respectively, are evaluated as

$$c_v = \left(\frac{\partial e}{\partial T} \right)_{v, X_i} = c_v^{ig} - K_1 T \left(\frac{\partial^2 a}{\partial T^2} \right)_{X_i} \tag{46}$$

$$c_p = \left(\frac{\partial h}{\partial T} \right)_{\mathrm{p}, X_i} = c_p^{ig} - R - K_1 T \left(\frac{\partial^2 a}{\partial T^2} \right)_{X_i} - T \frac{(\partial p/\partial T)^2_{v, X_i}}{(\partial p/\partial v)_{T, X_i}} \tag{47}$$

The speed of sound for a real fluid is given by

$$c^2 = \left(\frac{\partial p}{\partial \rho} \right)_{s, X_i} = \frac{\gamma}{\rho \kappa_T} \tag{48}$$

where γ is the specific heat ratio and κ_T is the isothermal compressibility defined as

$$\kappa_T = -\frac{1}{v}\left(\frac{\partial v}{\partial p} \right)_{T, X_i} \tag{49}$$

The specific heat ratio is linearized around temperature to eliminate the costly iterative procedure to determine temperature, and also to obtain other thermodynamic quantities which are functions of temperature.

2.5.4 Transport Properties

Transport quantities are evaluated based on the method due to Chung et al [39]-[40]. A power-law is used to approximate the temperature dependency:

$$\frac{\tilde{\mu}}{\tilde{\mu}_0} = \left(\frac{\tilde{T}}{T_0} \right)^{a_\mu} \tag{50}$$

$$\frac{\lambda}{\tilde{\lambda}_0} = \left(\frac{\tilde{T}}{T_0} \right)^{a_\lambda} \tag{51}$$

The compressible flamelet methodology discussed above is thermodynamically consistent in the entire flow path of a rocket engine (from oxidizer and fuel manifolds to the exit of the nozzle) and circumvents the need for any ad hoc compressibility corrections of the FPV model in Loci-STREAM.

2.5.4 Compressible Combustion Model

The compressible flamelet modeling capability presented here seamlessly handles all parts of the combustion domain, including the upstream fuel and oxidizer manifold sections, the combustion chamber and the highly compressible nozzle. In the classical low-Mach number flamelet implementations, the temperature, species, and density are assumed to depend only on the transported scalars (Z and C). However, when compressibility effects need to be taken into account, an overdetermined thermodynamic state arises from the use of the flamelet table with tabulated thermodynamics. On the one hand, the full thermodynamic state, at constant pressure, is defined within the flamelet table. On the other hand, the transport equations contain two thermodynamic variables, namely density and internal energy, which are also suffcient to fully characterize the thermodynamic equilibrium state of the fluid if the composition of the fluid mixture is known. In order to address this issue of the over-determined thermodynamic states, a strategy has been developed by Saghafian et al. [44] in the context of ideal gas flows to account for the pressure and temperature variations arising in supersonic combustion using the FPV approach. A similar approach is adopted here – the specific heat ratio is linearized around temperature to eliminate the costly iterative procedure to determine temperature, and also to obtain other thermodynamic quantities which are functions of temperature.

To properly account for compressibility, the underlying strategy rests on correcting the tabulated values in the flamelet table with the transported quantities based on the EoS used. Specifically, since PR-EoS is employed here, along with thermodynamic quantities needed for evaluation of the ideal gas thermodynamic quantities, parameters *a* and *b*, and the first and second derivatives of the parameter *a* with respect to temperature are needed for the calculations of the partial derivatives in the equations above which are required for the evaluation of the departure functions. However, the parameter *a*, along with its derivatives, is a function of both the species composition and the temperature, and thus may not be consistent with the temperature corresponding to the transported variables. The following procedure is adopted for the evaluation of the parameter *a* and its derivatives: the dependence of the parameter *a* on temperature is assumed to be a quadratic function as follows:

$$a = C_1 \tilde{T}^2 + C_2 \tilde{T} + C_3 \tag{52}$$

where the coefficients C_1, C_2, C_3 can be obtained from tabulated quantities:

$$C_1 = \frac{1}{2} \left(\frac{\partial^2 a}{\partial T^2} \right)_0 \tag{53}$$

$$C_2 = \left(\frac{\partial a}{\partial T} \right)_0 - 2 C_1 T_0 \tag{54}$$

$$C_3 = a_0 - C_1 T_0^2 - C_2 T_0 \tag{55}$$

where the subscript "0" indicates the stored baseline quantities in the table.

The first and second derivatives of the parameter *a* with respect to temperature can be determined by taking derivatives of Eq. (52); thus, the proposed model corresponds to a linear and a constant approximation to the first and second derivatives of *a*, respectively. Once the parameter *a* and its derivatives have been thus obtained, along with the parameter *b* and the gas constant *R*, all the partial derivatives which are needed for computing other thermodynamic quantities can be evaluated for a given

mixture, and therefore, the thermodynamic state is determined. Note that similar to the quadratic model given in Eq. (52), a linear model or a constant model for the parameter *a* can also be constructed based on the stored values in the table. The performance of the quadratic, linear, and constant models has been examined by Ma et al. [15] and the quadratic model was found to exhibit a superior performance in predicting the parameter *a* and its derivatives when temperature is away from the reference value. Moreover, this quadratic model performs very well in predicting other thermodynamic quantities [15], thus validating this approach.

The real-fluid energy is then evaluated as

$$\tilde{e} = \tilde{e}^{ig} + \tilde{e}^{dep} \tag{56}$$

where $\tilde{e}^{ig}$ and $\tilde{e}^{dep}$ are the ideal-gas and departure function values of the internal energy. The ideal-gas value including the chemical energy of the mixture is calculated with a linearized specific heat ratio:

$$\tilde{e}^{ig} = \tilde{e}_0^{ig} + \frac{\tilde{R}}{a_\gamma^{ig}} \ln\left(1 + \frac{a_\gamma^{ig}(\tilde{T} - T_0)}{\tilde{\gamma}_0^{ig} - 1}\right) \tag{57}$$

where $T_0, \tilde{e}_0^{ig}, \tilde{R}, a_\gamma^{ig}, \tilde{\gamma}_0^{ig}$ are parametrized with Z, Z''^2 and C, and stored in the flamelet table. The departure function is given by

$$\tilde{e}^{dep} = K_1\left[a - \tilde{T}\left(\frac{\partial a}{\partial T}\right)_{X_i}\right] \tag{58}$$

where Eqs. (52)-(55) are used to compute the parameters required for PR-EoS. To determine the primitive variables from the conservative variables, a bracketed secant method is used to obtain temperature given the transported pressure and internal energy. Following this, the density along with other thermodynamic quantities is evaluated as a function of the pressure and temperature.

The above compressible FPV (CFPV) approach focuses on the thermodynamics and no special modification is made for the chemistry part in the flamelet solver. Typically, in rocket engines, combustion takes place at high temperatures away from the real-fluid region where cryogenic temperatures exist. Combustion in typical rocket combustion chambers can be considered to occur at low-Mach conditions where compressibility effects are small. However, for the inert and equilibrium parts of the flows where the chemical source terms are not active, compressibility may play a critical role for predicting the behavior of the system locally – flows in the injectors and through the nozzles in rocket engines, for example. Therefore, in the fully compressible combustion model developed here for practical simulations, the flamelet table can be generated at conditions of the combustion chamber where combustion takes place, and discrepancies in temperature and pressure in other parts of the flows due to real-fluid effects and flow compressibility can be handled by the compressible FPV (CFPV) model described above.

The compressible flamelet progress variable (CFPV) model discussed above is thermodynamically consistent in the entire flow path of a rocket engine (from oxidizer and fuel manifolds to the exit of the nozzle) and obviates the need for ad hoc compressibility corrections of the FPV model in Loci-STREAM.

3 Results of a Validation Test Case

The first case used to validate the flamelet methodology is a single element GOX-GH2 shear coaxial injector with available wall heat flux data. This case is based on experiments conducted by Pal et al [45]. The experimental setup consists of a single element shear coaxial injector, a main cylindrical combustion chamber and two GOX/GH2 pre-burners which provide hot, oxidizer-rich and fuel-rich streams. The main chamber wall is instrumented with coaxial heat flux gauges which provide both temperature and heat flux profiles. The geometry for the simulations of this injector matches the internal

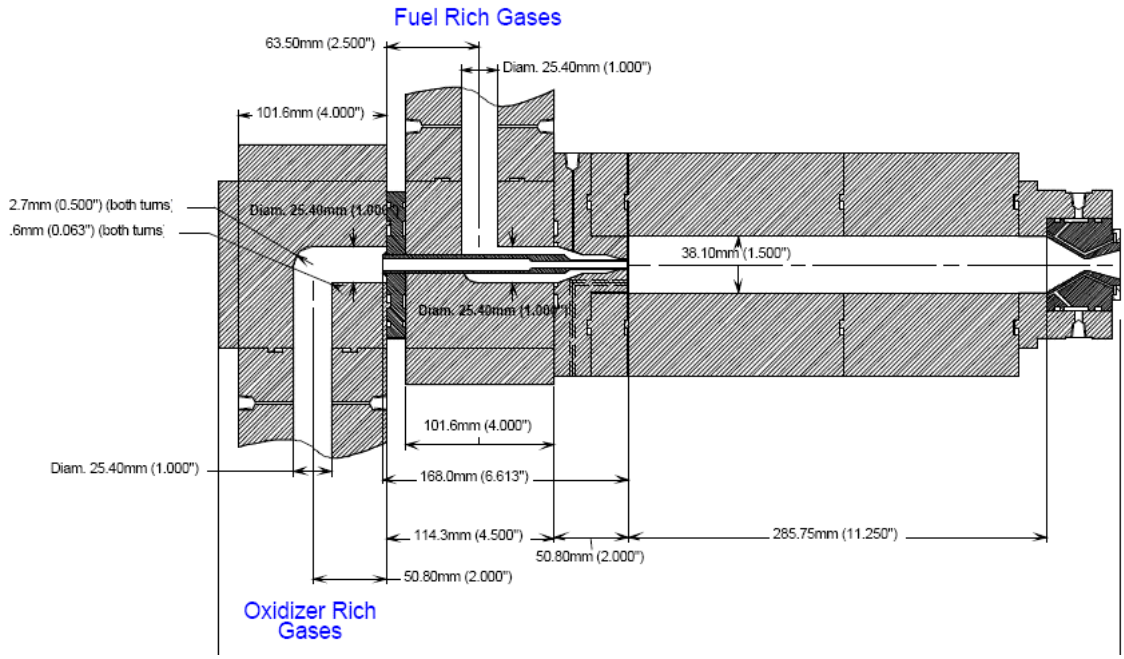

Figure 6. *Cross-section of the experimental geometry.*

injector element flow path of the hardware used in the experiments [45]. The experimental injector geometry with the fuel flow and oxidizer flow paths is shown in Figure 6. The geometry for the simulation consists of a single coaxial injector with a constant diameter chamber section and shown in Figure 7. Details of the experimental conditions are provided in Pal et al [45].

The key flow parameters and fluid properties are summarized in Table 1. The oxidizer stream contains 0.906 moles of oxygen, 0.0940 moles of water, and is injected at a temperature of 711 K. The fuel stream contains 0.857 moles of hydrogen, 0.143 moles of water, and is injected at 800 K. For the simulations, constant flow rates of 0.0904 kg/s (oxidizer) and 0.0331 kg/s (fuel) are specified at the respective inlets. No-slip conditions are applied at all wall surfaces. All of the injector wall surfaces are assumed to be adiabatic. The face of the combustion chamber and oxidizer post tip are assumed to be fixed at 755 K. The axial temperature distribution along the radial wall of the combustion chamber is specified using available experimental data. The nozzle temperature is assumed to be fixed at 510 K. The reference pressure for the computations is set at 5.2 MPa. At this pressure the bulk exit velocities of the injector are 154 m/s for the oxidizer stream and 764 m/s for the fuel stream.

As an initial test case, a relatively coarse 3D grid for the RCM1 injector was generated consisting of 6.8 million cells. Both RANS and DES simulations were conducted employing the CFPV model to test the stability and robustness of the overall algorithm. The SLAU convection scheme along with Crank-Nicolson time-stepping scheme was employed for these simulations. Figure 8 shows the 3D geometry as well as a representative DES result of the temperature field – an iso-surface of temperature equal to 3300K at one time instant is shown along with the temperature distribution on the walls of the combustor geometry. Figure 9 shows the contours of temperature and OH mass fraction, respectively, at one time instant.

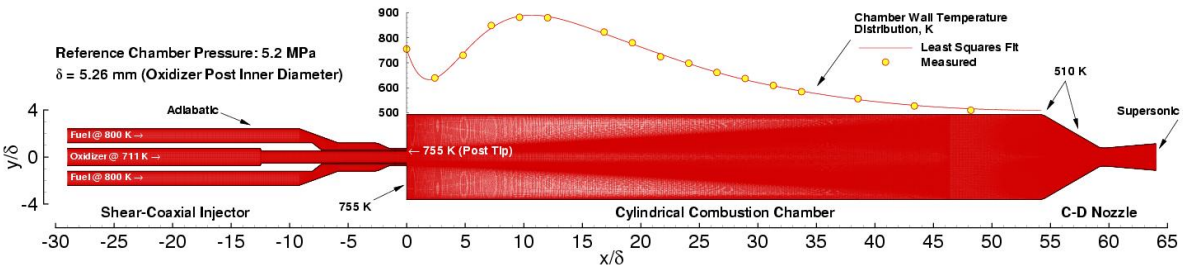

Figure 7. *Computational domain with the specified boundary conditions.*

	Oxidizer Stream	Fuel Stream
Stream Composition:		
Composition by Mass	0.945 (O_2) / 0.0550 (H_2O)	0.402 (H_2) / 0.598 (H_2O)
Composition by Volume	0.906 (O_2) / 0.0940 (H_2O)	0.857 (H_2) / 0.143 (H_2O)
Total Mass Flow Rate, kg/s	9.04×10^{-2}	3.31×10^{-2}
Reference Properties:		
Pressure, MPa	5.2	
Temperature, K	711	800
Density, kg/m^3	26.8	3.33
Specific Heat (C_p), J/kg·K	1110	
Ratio of Specific Heats	1.34	1.38
Dynamic Viscosity, Pa·s	3.62×10^{-5}	1.81×10^{-5}
Thermal Conductivity, W/m·K	0.0602	0.260
Kinematic Viscosity, m^2/s	1.35×10^{-6}	5.44×10^{-6}
Thermal Diffusivity, m^2/s	2.03×10^{-6}	10.8×10^{-6}
Sound Speed, m/s	513	1470

Table 1. *Key flow parameters and fluid properties for the RCM1 GOX-GH2 injector.*

As the next step, a mesh refinement study was conducted at NASA to ensure that the CFD solution was independent of the mesh spacing. The hybrid-unstructured mesh employed for the simulations was optimized to produce accurate, engineering quality wall heat flux results while limiting the volume cell

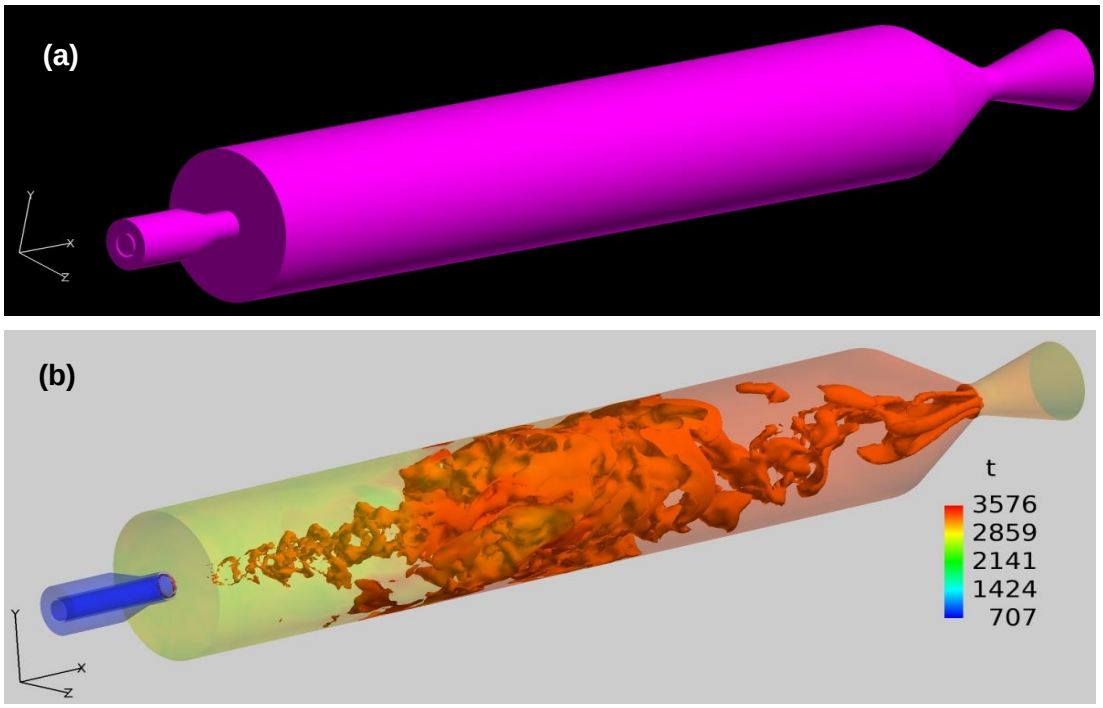

Figure 8. *3D coarse-grid DES simulation of RCM1 injector: (a) 3D geometry; (b) Iso-surfaces of T=3300K and boundary contours of temperature at one instant.*

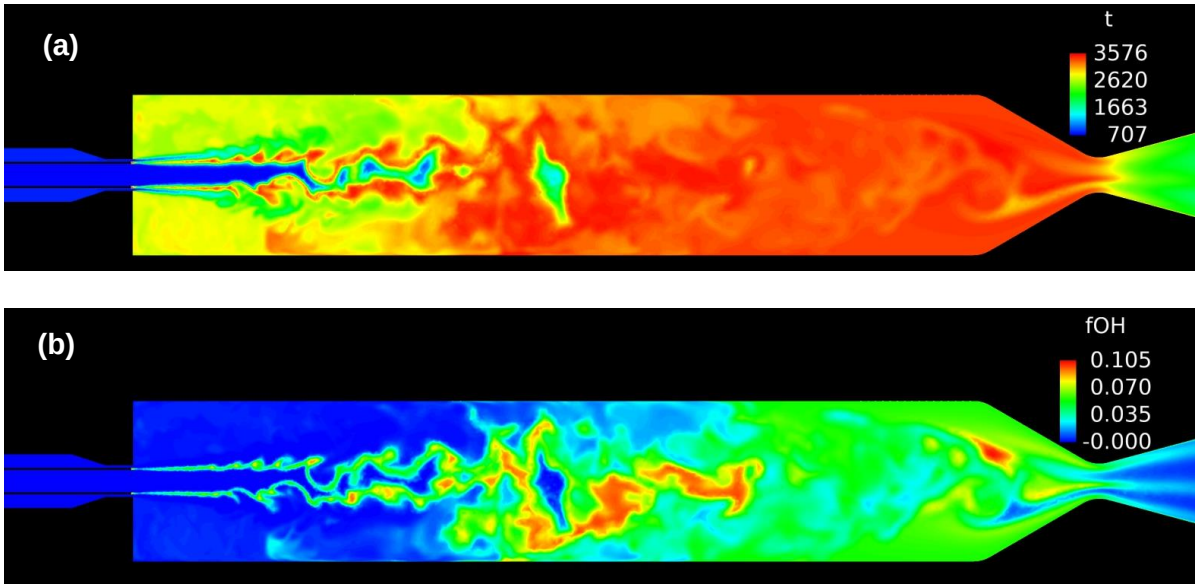

Figure 9. *3D coarse-grid DES simulation of RCM1 injector using the CFPV model: (a) temperature and (b) OH mass fraction at one time instant.*

count to approximately 30 million to facilitate a reasonable computational turn-around time. The mesh density is the highest near the surface of the oxidizer post tip and along the adjacent surfaces. The mesh was also refined along the shear layer region. To enable an accurate simulation of heat transfer between the chamber gas and the wall, the y+ of the near-wall cells is limited to a value of 0.5 throughout most of the chamber.

Figure 10 shows the wall heat flux results of simulations from the two flamelet models in Loci-STREAM: (a) the FPV model with beta-PDF closure (labelled STREAM-FPV-Beta) and (b) the CFPV model with thickened flame closure (labelled STREAM-CFPV-TF). plotted against the experimental data and other CFD simulations results found in the literature. Due to the relatively simple complexity of hydrogen-oxygen chemistry mechanisms, direct modeling of reactions with laminar finite chemistry is feasible for this application. Results from two studies using finite rate chemistry models are shown in Figure 10, namely: (a) the simulation by Tucker et al. [46]– labelled FRC-RANS-Tucker in Figure 10 – which used laminar finite rate chemistry and steady-state RANS model on an axisymmetric, 400 thousand cell mesh, and (b) the simulation conducted by Oefelein [46] – labelled FRC-LES-Oefelein

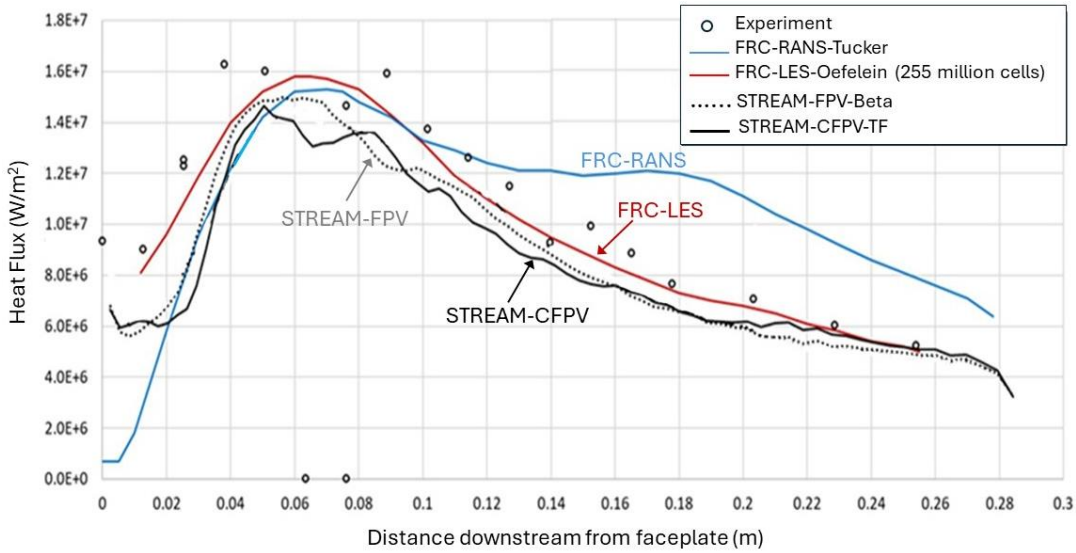

Figure 10. *Wall heat transfer for GOX/GH2 injector: comparison with experimental data.*

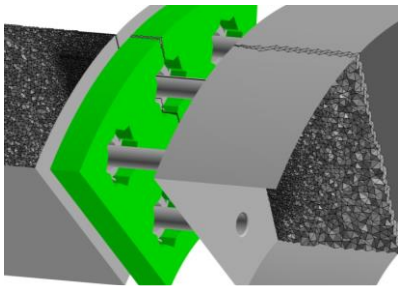

Five-element sector of GOX-RP1 injector: using 130 million grid cells and 2000 CPUs. Loci-STREAM's overset mesh capability was utilized to combine the components into a 5-element sector computational domain.

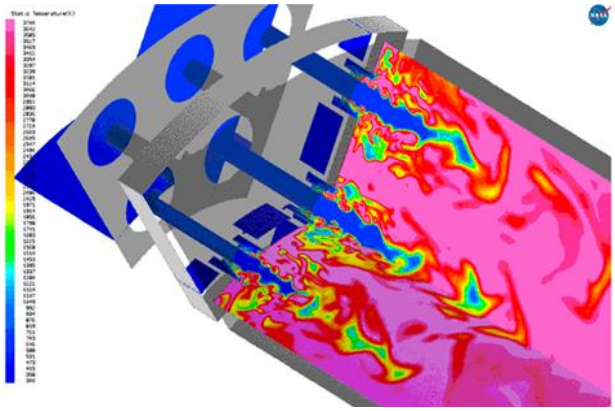

GOX-RP1 injector: instantaneous temperature field.

Figure 11. *Application of the compressible flameless progress variable (CFPV) model in Loci-STREAM to (a) GOX-RP1 injector simulation [47].*

in Figure 10 – which used finite rate chemistry, time-accurate LES, and a specialized sub-grid scale model on a three-dimensional, 255 million cell mesh. The wall heat transfer result from the FRC-LES-Oefelein simulation provides the best match with the experimental data in terms of the location and magnitude of the peak heat release as well as the profile downstream. The FRC-RANS-Tucker simulation overpredicts the wall heat transfer profile downstream of the peak location. Both flamelet-based models, namely, the STREAM-FPV-Beta and STREAM-CFPV-TF models, capture the general physics and the variation of heat flux down the chamber. However, both flamelet models underpredict the wall heat flux compared to the experiment by about 10-15% of the reported values in the data. The flamelet simulations also underpredicted the peak heat flux value and the values downstream by about 10%.

4 Sample Rocket Engine Injector Simulations

The turbulent combustion modeling capability in Loci-STREAM based on the flamelet methodology has been employed at NASA for a variety of rocket combustor simulations. Figure 11shows a five-element sector of a GOX-RP1 injector using 130 million cells and more than 2000 CPUs on the NASA Pleaides supercomputing cluster. Loci-STREAM's overset mesh capability was utilized to combine the components into a 5-element sector computational domain [47]. Finally, sample results from CFD simulations of modern oxygen-methane engines using Loci-STREAM conducted to support in-space propulsion development projects by Richardson [48] at NASA are presented in Figure 12. The following sample large-scale simulations are presented:

(a) Oxygen-methane engine design concept using shear flow injector elements:

This case involves a concept oxygen-methane engine design using shear flow injector elements. The goal of this simulation was to extract heat flux distribution to chamber walls for a range of conditions to ensure that enough heat was extracted from the chamber walls to drive the turbine. The CFPV model was utilized to enable efficient use of a large mesh and complex geometry. As seen in Figure 12(a), the blue iso-surface shows where the flame rapidly transitions from majority unburned O2 and CH4 propellant to majority combustion products such as CO2, CO and H2O. The green-yellow wall surface plot shows contours of heat flux into the chamber wall. The hardware was designed to have higher heat flux at the aft end (right side) of the chamber. Traditionally, empirically derived design tools are not capable of accurately predicting this type of axial heat flux distribution down the chamber wall. The CFD-predicted wall heat flux was used to develop the turbine power cycle.

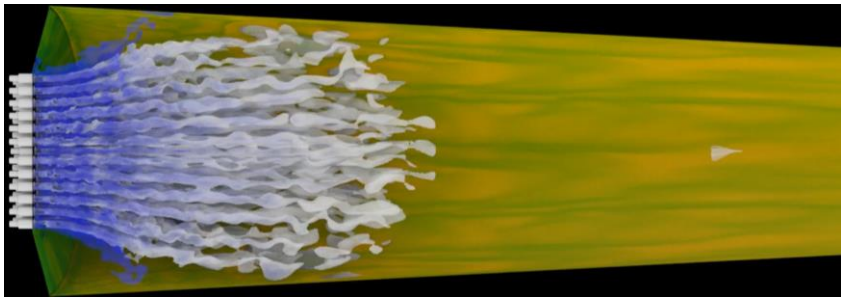

(a) CH4-GOX combustion inside a concept engine chamber using shear flow injector elements; simulation by Richardson [48].

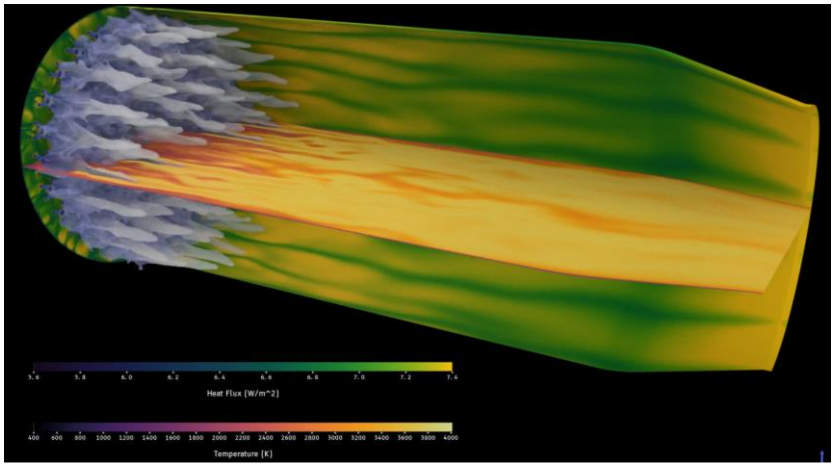

(b) CH4-GOX combustion inside a concept engine chamber using impinging injector elements (100 injector elements, 600+ million grid cells); simulation conducted by Richardson [48].

Figure 12. *Combustion modeling of oxygen-methane engine design concepts using the compressible flamelet progress variable (CFPV) model in Loci-STREAM [48].*

(b) Oxygen-Methane engine design concept using impinging flow injector elements:

The next case involves a concept oxygen-methane engine design using impinging flow injector elements. The goal of this simulation was to quantify the heat release distribution in the primary combustion zone to quantify potential combustion instability modes. The CFPV model was employed to enable efficient use of a large mesh and complex geometry. This combustion simulation involves more than 100 injector elements and more than 600 million volume cells. As seen in Figure 12(b), the blue iso-surface shows where the flame rapidly transitions from majority unburned O2 and CH4 propellants to majority combustion products such as CO2, CO and H2O. The cross-section shows temperature contours. The combustion gas temperature rapidly increases just downstream of the blue iso-surface which is the vigorous combustion zone. The green-yellow wall surface plot shows contours of heat flux into the chamber wall. This simulation showed that the impinging injector elements force rapid combustion of the propellants as indicated by the relatively short persistence of the blue iso-surface down the chamber. The CFD simulation was able to provide the time lag parameter which is not well quantified in traditional combustion stability analysis methods for this injector type.

3 Conclusion and Future Work

A computational tool capable of modeling unsteady turbulent combustion using a compressible flamelet methodology has been developed which provides a high-performance, high-fidelity simulation capability to enable accurate, fast and robust simulation of unsteady turbulent, reacting flows in rocket engines. The classical flamelet methodology has been extended to handle both ideal gases and real

fluids. The thermodynamics for ideal-gas values is modeled by a linearized specific heat ratio model. Real fluid effects are modeled with the cubic Peng-Robinson equation of state (PR EoS). The parameters needed for the PR EoS are pre-tabulated for the evaluation of departure functions and a quadratic expression as a function of temperature is used to recover the attraction parameter away from the reference temperature. The present Compressible Flamelet Progress Variable (CFPV) methodology developed in Loci-STREAM is able to account for pressure and temperature variations from the baseline table and is thermodynamically consistent in the entire flow path of a rocket engine (from oxidizer and fuel manifolds to the exit of the nozzle) and circumvents the need for ad hoc compressibility corrections of the standard Flamelet Progress Variable (FPV) model. These enhancements in Loci-STREAM have yielded higher fidelity and a more reliable analytical/design capability relative to the existing capability for turbulent reacting flows in rocket engines.

4 Acknowledgements

Funding support from NASA Marshall Space Flight Center (MSFC) is gratefully acknowledged. The authors thank Brian Richardson and Jeffrey West of NASA MSFC for technical discussions as well as for providing sample results of simulations conducted at NASA using Loci-STREAM.

References

[1] Thakur, S. and Wright, J., "An All-Speed Solver for Unsteady Reacting and Non-Reacting Flows Using a Rule-Based Framework," 42nd AIAA Fluid Dynamics Conference, #AIAA-2012-3254 (2012).

[2] Pitsch, H., "Large-Eddy Simulation of Turbulent Combustion," Annu. Rev. Fluid Mech, Vol. 38 (2006).

[3] Pitsch, H., Chen, M., and Peters, N., "Unsteady Flamelet modeling of turbulent hydrogen-air Diffusion Flames," Twenty-Seventh Symposium on Combustion, The Combustion Institute (1998).

[4] Wu, H., See, Y. C., Wang, Q., and Ihme, M., "A Pareto-Efficient Combustion Framework with Submodel Assignment for Predicting Complex Flame Configurations," Combust. Flame, Vol. 162, No. 11, pp. 4208-4230 (2015).

[5] S. Thakur, J. Wright, C. Neal and M. Ihme, "Development of a Fidelity-Adaptive Combustion Modeling Framework in a Rule-Based All-Speed Implicit Flow Solver," Paper #6.2022-1203, AIAA SciTech Forum (2022).

[6] Wu, H. and Ihme, M., "Compliance of Combustion Models for Turbulent Reacting Flow Simulations," Fuel, Vol. 186, pp. 853-863 (2016).

[7] Pierce, C. and Moin, P., "Progress-Variable Approach for Large-Eddy Simulation of Non-Premixed Turbulent Combustion," J. Fluid Mech., Vol. 504, pp. 73-97 (2004).

[8] Ihme, M., Cha, C., and Pitsch, H., "Prediction of Local Extinction and Re-Ignition Effects in Non-Premixed Turbulent Combustion Using a Flamelet/Progress Variable Approach," P. Comb. Inst., Vol. 30, pp. 793-800 (2005).

[9] S. Thakur, M. Ihme and J.P. Hickey, "Turbulent Combustion CFD Solver in a Rule-Based Framework Using a Variable Pressure Flamelet Model," 11th AIAA/ASME Joint Thermophysics and Heat Transfer Conference, #AIAA-2014-2253 (2014).

[10] S. Thakur, J. Wright, M. Ihme, "Compressible Flamelet Model in a Rule-Based Turbulent Combustion Solver," 54th AIAA Aerospace Sciences Meeting, AIAA SciTech, #AIAA-2016-1838 (Jan 2016).

[11] Richardson, B.R. and Kenny, J., "3-D CFD Simulation and Validation of Oxygen-Rich Hydrocarbon Combustion in a Gas-Centered Swirl Coaxial Injector using a Flamelet-Based Approach," JANNAF Propulsion Meeting, Nashville, TN, June 1-5 2015.

[12] Westra, D.G., West, J.S. and Richardson, B.R., "Unsteady Three-Dimensional Simulation of a Shear Coaxial GO2/GH2 Rocket Injector with RANS and Hybrid-RAN-LES/DES Using Flamelet Models," JANNAF Propulsion Meeting, Nashville, TN, June 1-5 2015.

[13] K. E. Braman & J. S. West "Validation of a Flamelet model with Non-Adiabatic Surfaces for Rocket Combustion Chamber Simulations," JANNAF Propulsion Meeting, 65th JPM / PIB / 12th MSS / 10th LPS / 9th SPS Joint Subcommittee Meeting, Long Beach, CA, May 2018.

[14] Richardon, B.R., Braman, K. and Longmire, N., "Efficient Rocket Chamber Combustion Analysis Using a Compressible Thickened-Flame Flamelet Model Approach," JANNAF Meeting, Huntsville, AL (2022).

[15] Ma, P.C., Banuti, D.T. and Ihme, M., "Numerical Framework for Transcritical Real-Fluid Reacting Flow Simulations Using the Flamelet Progress Variable Approach," AIAA-2017-0143 (2017).

[16] Luke, E.A., "LOCI: A Deductive Framework for Graph-Based Algorithms," *Third International Symposium on Computing in Object-Oriented Parallel Environments*, edited by S. Matsuoka, R. Oldehoeft and M. Tholburn, No. 1732 in Lecture Notes in Computer Science, Springer-Verlag, pp 142-153 (1999).

[17] Patankar, S. V., Numerical Heat Transfer and Fluid Flow, Hemisphere, Washington, DC (1980).

[18] Rhie, C.L. and Chow, W.L., "A Numerical Study of the Turbulent Flow Past an Isolated Airfoil with Trailing Edge Separation," AIAA Journal, 21: 1525-1532 (1983).

[19] Shyy, W., Thakur, S. S., Ouyang, H., Liu, J. and Blosch, E., Computational Techniques for Complex Transport Phenomena, Cambridge Univ. Press, NY (1997).

[20] Liou, M., "A sequel to AUSM: AUSM+," Journal of Computational Physics 129 (1996) pp 364–382 (1996).

[21] Shima, E. and Kitamura, K., "On New Simple Low-Dissipation Scheme of AUSM-Family for All Speeds," AIAA 2009-136, 47th AIAA Aerospace Sciences Meeting, (2009).

[22] Kitamura, K., and Shima, E., "Towards Shock-Stable and Accurate Hypersonic Heating Computations: A New Pressure Flux for AUSM-Family Schemes," J. Comput. Phys., 245, pp. 62–83 (2013).

[23] Launder, B.E. and Spalding, D.B., "The Numerical Computation of Turbulent Flows," Comp. Meth. App. Mech. and Engg., Vol. 3, Issue 2, pp 269-289 (1974).

[24] Wilcox, D.C., Turbulence Modeling for CFD, DCW Ind., La Canada, CA (1998).

[25] Menter, F.R., "Two-Equation Eddy Viscosity Turbulence Models for Engineering Applications," *AIAA Journal*, Vol. 32, No. 8, pp 1598-1605 (1994).

[26] Smagorinsky, J., "General circulation experiments with primitive equations. I. The basic experiment," Monthly Weather Review, Vol. 91, pp. 99-164 (1963).

[27] Nicoud, F. and Ducros, F., "Subgrid-scale stress modelling based on the square of the velocity gradient tensor," Flow, Turbulence and Combustion 62: 183–200 (1999).

[28] Spalart, P.R., "Detached-Eddy Simulation," *Ann. Rev. Fluid Mech.*, Vol. 41, pp 181-202 (2009).

[29] Shur, M.L., Spalart, P.R., Strelets, M.K. and Travin, A.K., "A Hybrid RANS-LES Approach with Delayed-DES and Wall-Modelled LES Capabilities," *Int. J. Heat Fluid Flow*, Vol. 29, pp 1638-1649 (2008).

[30] Nelson, C.C. and Nichols, R.H., "Application of Hybrid RANS/LES Turbulence Models," *AIAA Paper 2003-0083* (2003).

[31] Peters, N., "Turbulent Combustion," Cambridge University Press (2000).

[32] Cutrone, L., Palma, P. D., Pascazio, G., and Napolitano, M., “A RANS Flamelet/Progress-Variable Method for Computing Reacting Flows of Real-Gas Mixtures," Comput. Fluids, Vol. 39, No. 3, 2010, pp. 485-498 (2010).

[33] Giorgi, M. G. D., Sciolti, A., and Ficarella, A., “Application and Comparison of Different Combustion Models of High Pressure LOX/CH4 Jet Flames," Energies, Vol. 7, pp. 477-497 (2014).

[34] Peng, D.-Y. and Robinson, D. B., “A new two-constant equation of state,” Ind. Eng. Chem. Res., Vol. 15, No. 1, pp. 59-64 (1976).

[35] Ely, J. F. and Hanley, H., “Prediction of transport properties. 1. Viscosity of fluids and mixtures,” Ind. Eng. Chem. Res., Vol. 20, No. 4, pp. 323-332 (1981).

[36] Ely, J. F. and Hanley, H., “Prediction of transport properties. 2. Thermal conductivity of pure fluids and mixtures,” Ind. Eng. Chem. Res., Vol. 22, No. 1, pp. 90-97 (1983).

[37] Harstad, K. G., Miller, R. S., and Bellan, J., “Efficient high-pressure state equations,” AIChE J., Vol. 43, No. 6, pp. 1605-1610 (1997).

[38] Poling, B.E., Prausnitz, J.M., and O'Connell, J.P., The properties of gases and liquids, McGraw-Hill New York, (2001).

[39] Chung, T.H., Lee, L.L., and Starling, K.E., “Applications of kinetic gas theories and multiparameter correlation for prediction of dilute gas viscosity and thermal conductivity,” Ind. Eng. Chem. Res., Vol. 23, No. 1, pp. 8-13 (1984).

[40] Chung, T. H., Ajlan, M., Lee, L. L., and Starling, K. E., “Generalized multiparameter correlation for nonpolar and polar fluid transport properties,” Ind. Eng. Chem. Res., Vol. 27, No. 4, pp. 671-679 (1988).

[41] Legier, JP, Poinsot, T and Veynante, D, “Dynamically thickened flame LES model for premixed and non-premixed turbulent combustion,” Center for Turbulence Research Proceedings of the Summer Program, p 157-168 (2000).

[42] Colin, O., Ducros, F, Veynante, D and Poinsot, T, “A thickened flame model for large eddy simulations of turbulent premixed combustion,” Physics of Fluids 12, pp 1843-1863 (2000).

[43] Vreman, AW, Albrecht, BA, van Oijen, J.A, de Goey, LPH, Bastiaans, RJM, “Premixed and nonpremixed generated manifolds in large-eddy simulation of Sandia flame D and F,” Combustion and Flame 153, pp 394–416 (2008).

[44] Saghafian, A., Terrapon, V. E., and Pitsch, H., “An Efficient Flamelet-Based Combustion Model for compressible Flows,” Combust. Flame, Vol. 162, No. 3, 2015, pp. 652{667.

[45] Pal, S., Marshall, W., Woodward, R. and Santoro, R., “Wall heat flux measurements for a uni-element GO2/GH2 shear coaxial injector,” 2006. Third International Workshop on Rocket Combustion Modeling, Paris, France, March, 13-15 (2006).

[46] Tucker, P.K., Menon, S., Merkle, C.L., Oefelein, J.C. and Yang, V., “Validation of High-Fidelity CFD Simulations for Rocket Injector Design,” 44th AIAA/ASME/SAE/ASEE Joint Propulsion Conference, Hartford, CT (2008).

[47] West, J., NASA/MSFC ER42, Private Communication.

[48] B. Richardson, “Inside the Fire: Simulating Combustion of Oxygen-Methane Fuel for Spacecraft Applications,” 2023 Supercomputing Conference, Denver, CO (2023).